Segmenting Continuous but Sparsely-Labeled Structures in Super-Resolution Microscopy Using Perceptual Grouping

Jiabing Li(✉), Camille Artur, Jason Eriksen, Badrinath Roysam, and David Mayerich

University of Houston, Houston, USA
jiabingli601@hotmail.com

Abstract. Super Resolution (SR) microscopy leverages a variety of optical and computational techniques for overcoming the optical diffraction limit to acquire additional spatial details. However, added spatial details challenge existing segmentation tools. Confounding features include protein distributions that form membranes and boundaries, such as cellular and nuclear surfaces. We present a segmentation pipeline that retains the benefits provided by SR in surface separation while providing a tensor field to overcome these confounding features. The proposed technique leverages perceptual grouping to generate a tensor field that enables robust evolution of active contours despite ill-defined membrane boundaries.

Keywords: Super resolution · Segmentation · Perceptual grouping · Tensors · Contours

Super resolution (SR) microscopy [24] encompasses a set of imaging techniques that overcome the diffraction limit [8] of traditional microscopes. SR imaging enables high-resolution microscopy, enabling biologists to probe tissue structure at the nanometer scale. In recent years, a number of novel approaches have been employed to circumvent the diffraction limit, including expansion microscopy (ExM) [2,5], stimulated emission depletion microscopy (STED) [25], photo activation localization microscopy (PALM) [9], stochastic optical reconstruction microscopy (STORM) [19] and structured illumination microscopy (SIM) [7].

SR provides greater spatial detail, enabling differentiation of individual protein clusters and separating tightly packed membranes (Fig. 1). While these additional features provide important details for understanding tissue structure, they challenge automated segmentation algorithms. For example, cellular and nuclear membranes are often identified by labeling embedded proteins, resulting in non-continuous punctate boundaries (Fig. 1). Algorithms commonly used for traditional microscopy, such as the FARSIGHT Toolkit [1] produce over-segmented

A. L. Martel et al. (Eds.): MICCAI 2020, LNCS 12265, pp. 141–150, 2020.
https://doi.org/10.1007/978-3-030-59722-1_14

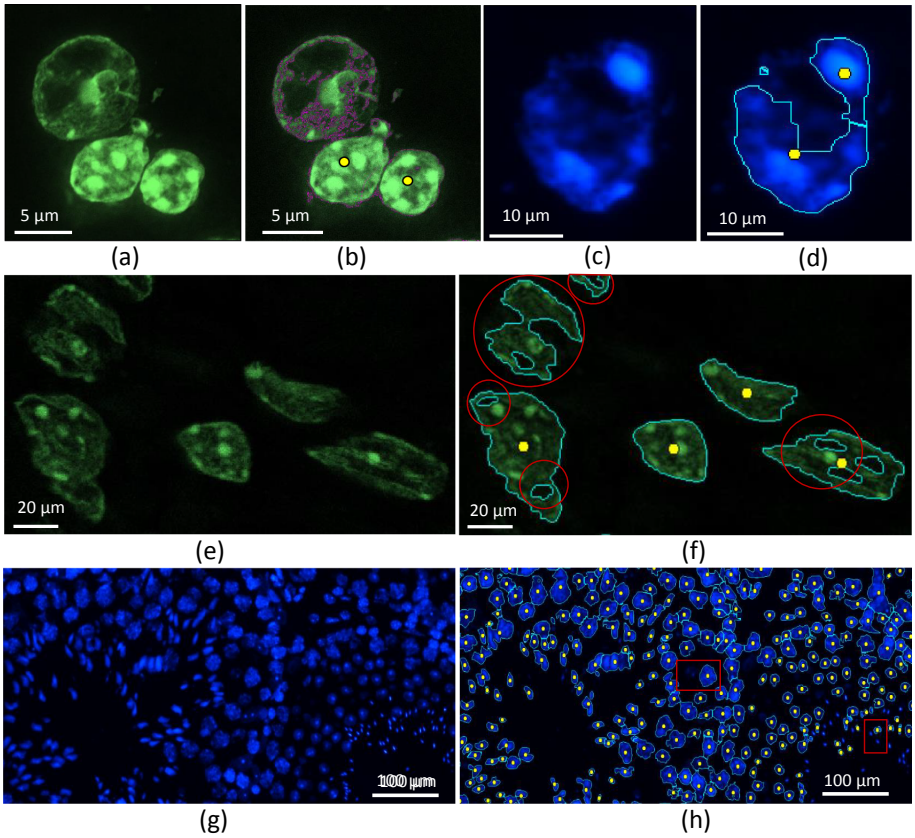

Fig. 1. FARSIGHT segmentation results on mouse brain(a, b, e, f) and kidney(c, b) histological nuclear staining using STED (a, b), using ExM (c, d, g, h), and high-resolution confocal microscopy (e, f).

results. Other challenges include (1) heterogeneous cell shapes, (2) contrast disparities, and (3) overlapping/clustered cells and nuclei. **In general, enhanced resolution provides additional spatial detail while making surfaces less clearly defined.**

In this paper, we propose a novel segmentation method *localization-reinforced perceptual grouping* (LRPG) that constructs a tensor-based [10] representation of the image and then refines this field leveraging perceptual grouping methods [15]. The resulting tensor field forms the basis for a more robust SR segmentation. Our approach maintains the coherence of punctate surfaces as well as the desired benefits of surface separability provided by SR imaging. Performance is tested on SR images acquired using expansion microscopy (ExM) [2] and stimulated emission depletion (STED) [25]. Performance benchmarks are compared to the current state-of-the-art in cell and nuclear segmentation, including FARSIGHT [1], modular interactive nuclear segmentation (MINS) [13], and TIMING 2.0 [14].

Our perceptually-based approach improves the performance of active contours, such as level set, and provides a significant benefit over existing algorithms for SR images.

1 Localization-Reinforced Perceptual Grouping

Our proposed LRPG framework is shown as Fig. 2, which includes four main steps: cell centroid detection, tensor voting, level set evolution, and watershed segmentation. We first identify cell positions using iterative voting [20], which requires an initial estimate of cell radius. We then calculate and refine a tensor field used to guide contours through high-frequency features in the image. This refinement is based on optimizing the angular discrepancy between the primary tensor direction and cell centroids. Cell contours are identified using a level set method evolved from the set of centroids and guided by the refined tensor field. Finally, watershed method is applied to separate connected cells.

1.1 Cell Seeds Detection

A GPU-based iterative voting method [20] is used to quickly calculate candidate points representing cell positions. We initialize the voting using the image gradient and apply iterative voting. The voting fields are refined to produce a set of candidate seeds (Fig. 3). A threshold is specified across the entire voting data to select candidate cell positions. Note that iterative voting requires an estimate of the cell radius as input. Since cell sizes can cover a wide range, we apply scale-space sampling using multiple iterative voting with different radius parameters. The voting images are added together and smoothed with a Gaussian filter ($\sigma = 5$) to merge multi-detected cell positions. Finally, a single iterative voting step is applied to this final image to extract the set of final cell centroids.

1.2 Localization Reinforced Tensor Voting

Tensor voting [12,16,17] is an algorithm for identifying "salient" structures in multi-dimensional data. This approach uses local features to reinforce global structure [6]. We leverage this approach to (1) reconstruct cell contours, and (2) extract refined tensor field flow as force flow for level set segmentation and gradient flow for watershed segmentation.

A Canny edge detector [21] is applied to identify candidate contour features defining cell boundaries. These contours are encoded using ball tensors when construct original tensor field and then iteratively refined using tensor voting [16]. After each voting iteration, the tensor field is decomposed into eigenvalues λ_1, λ_2 and their corresponding eigenvectors e_1, e_2 [10,17], which is defined as:

$$T = \lambda_1 e_1 e_1^T + \lambda_2 e_2 e_2^T = (\lambda_1 - \lambda_2) e_1 e_1^T + \lambda_2 (e_1 e_1^T + e_2 e_2^T), \tag{1}$$

where $(\lambda_1 - \lambda_2) e_1 e_1^T$ describes a stick tensor T_S and $\lambda_2 (e_1 e_1^T + e_2 e_2^T)$ describes a ball tensor T_B. Each feature is characterized by its curve saliency $(\lambda_1 -$

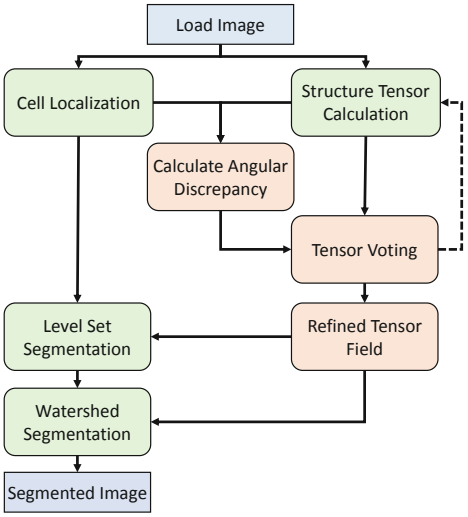

Fig. 2. Pipeline of localization-reinforced perceptual grouping. Input image are processed into four main steps: cell seeds extraction, cell saliency feature extraction from tensor voting, binary mask extraction from level set segmentation and final using seeds based watershed methods to segment every single cell.

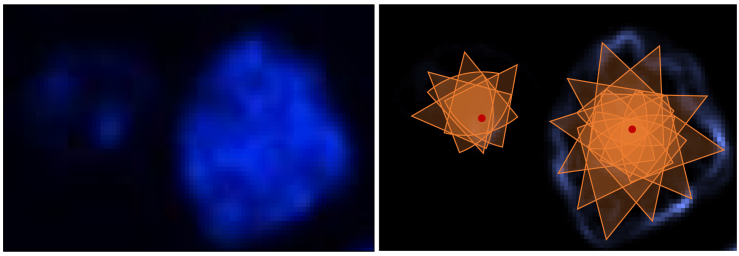

Fig. 3. Iterative voting for cell seeds identification [20]. (a) Input image. (b) Calculate the gradient of the input image and each non-zero point of the gradient image can be a voter. Then calculate voting area of voter and integrate all votes from voters. Local maximum algorithm is applied to extract cell positions candidates.

λ_2) with orientation e_1, and point saliency λ_2 with no preferred orientation (Fig. 4(a)). We apply a threshold (usually 0.05) on curve feature $(\lambda_1 - \lambda_2)$ to remove useless contour sides. Salient cell contours are then reconstructed by iterative tensor voting (Fig. 5).

We then implement a novel localization-reinforced tensor voting method to generate and refine a field for contour evolution. A new field $\mathbf{S}(x, y)$ is generated by calculating the structure tensor at each point. We then calculate the angular discrepancy $R(x, y)$ between cell centroids and principal eigenvectors $\mathbf{e}_1(x, y)$

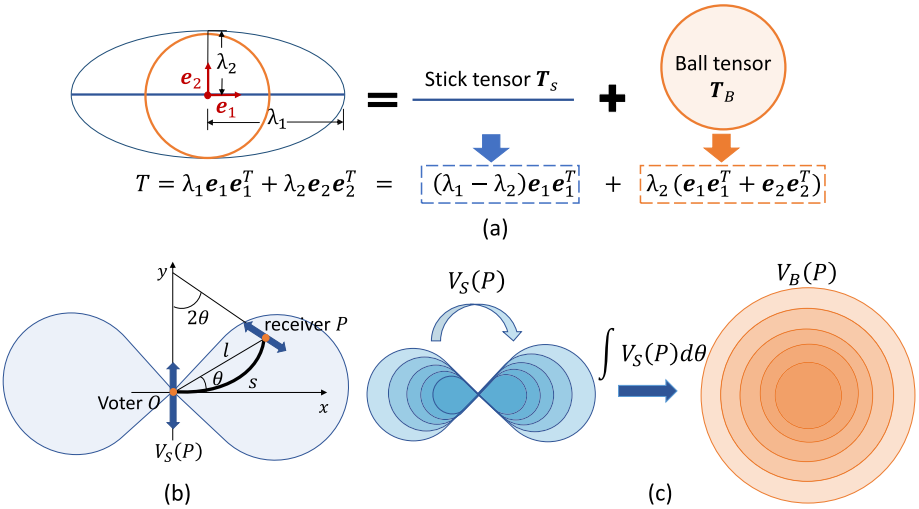

Fig. 4. (a) Tensor decomposition into a stick tensor and ball tensor. (b) Stick tensor voting field calculation. O is the voter and P is a receiver, s is the arc length, and l is OP length, θ is the angle between the tangent to the osculating circle at the voter and the line going through the voter and receiver. Voting value is based on saliency decay function: $V_S(l, \theta, \sigma) = e^{\frac{s^2 + ck^2}{\sigma^2}}$,, where $s = \frac{\theta l}{sin\theta}, k = \frac{2sin\theta}{l}$. Voting value is zero if θ larger than $\pi/4$. (c) Ball voting field is an integration of stick tensor voting field.

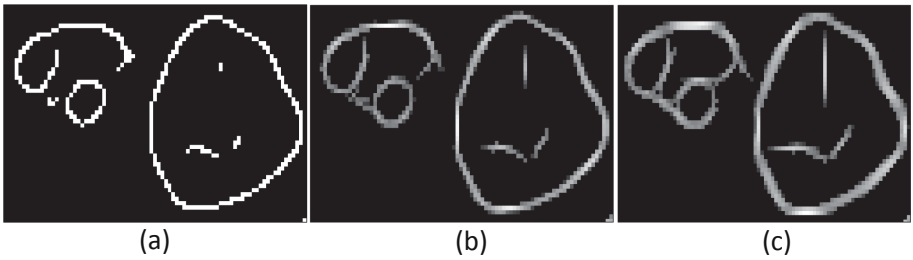

Fig. 5. Cell contours reconstruction from iterative tensor voting. (a) Original cell curve after applying a Canny detector. (b) Cell contours after one time tensor voting. (c) Cell contours after two times tensor voting.

of $\mathbf{S}(x, y)$ by computing their dot product with the gradient of the centroid's Euclidean distance field $\mathbf{D}(x, y)$:

$$R(x, y) = \left| \frac{\mathbf{e}_1(x, y) \cdot \nabla \mathbf{D}(x, y)}{||\mathbf{e}_1(x, y) \cdot \nabla \mathbf{D}(x, y)||} \right| \tag{2}$$

The angular discrepancy $R(x, y)$ can be thought of as a scalar value to quantify each tensor's reliability. Then we set a threshold t_r on R to force unreliable voters' value to zero (our experiments use $t_r = 0.8$).

Then for each voting iteration, the total number of votes received at a pixel i is given by:

$$T_{n+1} = T_n + R \sum_{i \varepsilon \omega} V(i), \tag{3}$$

where the $V(i)$ means the total voting at pixel i integrated from neighbor voters. We repeat the step of localization reinforced tensor voting until most (usually 90%) tensors are recognized as reliable tensors, which means small angular discrepancy with seeds. Finally, we decompose the final refined tensor field T_N to extract eigen vector e_{1N} as cell contours expansion flow. After the localization reinforced tensor voting, we can see the original messed tensor field (Fig. 6(c)) becomes the refined tensor field (Fig. 6(d)), in which most tensors are aligned to point to seeds. Most importantly, the tensor field still keeps the original cell shapes.

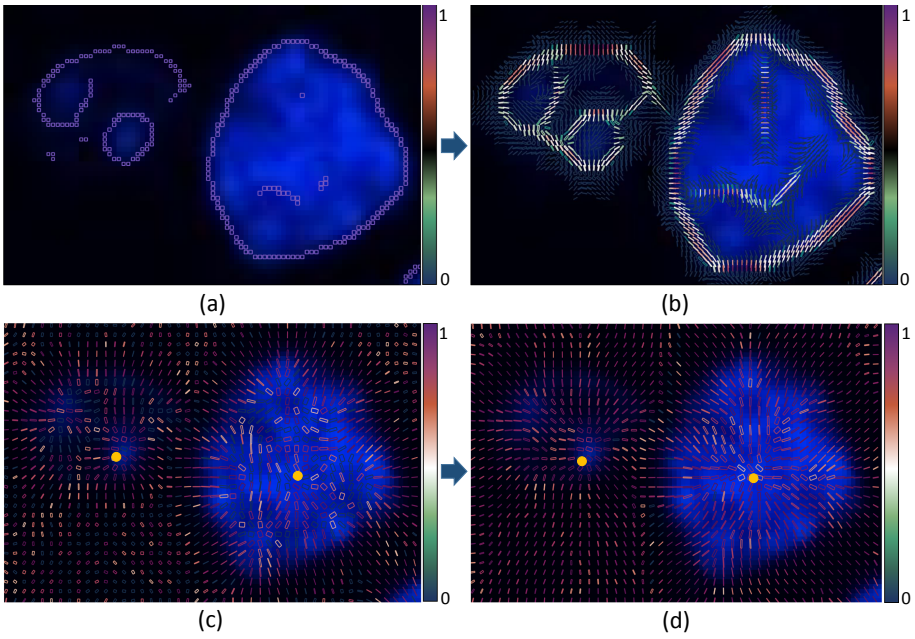

Fig. 6. Tensor field refining. (a) Original encoded tensor field of Canny edge using ball tensor. (b) Cell contours tensor field after iterative tensor voting. (c) Original mess tensor field encoding using image gradient. (d) Refined tensor field after localization reinforced tensor voting. Color bars indicate tensor reliability. (Color figure online)

1.3 Level Set Contour Evolution

Level set methods [18,22] are commonly used to solve curve evolution problems with potential topological changes, such as splitting and merging. This approach

calculates the evolution of an embedded (2D) curve within a higher-dimensional (3D) space. The curve is initialized as a point at each cell centroid and propagated along a velocity field specified by the refined tensor field using Euler integration to solve the resulting partial differential equation (PDE) [4,11]. Iterative voting provides high confidence cell centroids used as initial contours. The eigenvector $\mathbf{e}_1(x, y)$ provides the outward gradient flow and $\nabla I'$ provides an additional inward force. The level set contour moves outward following $\mathbf{e}_1$ until balanced by the inward force to achieve a minimum energy state.

Our level set based on refined tensor field performs significantly better than a traditional level set approach based on gradient. Due to the velocity field design, traditional level set evolution often stops at local minima. Since refined tensor field provide continue flow from cell centers to cell boundaries, it can help level set evolution propagate over dim signal part to real cell boundaries.

1.4 Watershed Segmentation

Watershed algorithm [23] is used to separate connected cells. Due to too many local minima problem in traditional gradient-descent algorithms, watershed often results in over-segmentation [3]. From the refined tensor field, we can extract the smoothing gradient field to filter out local minima. So it can fix over-segmentation efficiently (Fig. 8). To prove that, we reconstruct image I' using the Poisson Reconstruction method [26]. In Fig. 7(a), we can see that the reconstructed cell has the highest intensity in its center with intensity decreasing gradually from center to boundaries. The gradient from I' could remove the impact of noise and quantization errors in watershed. It also can be seen as a refined cell distance field keeping the original cell shape. Combining extracted binary mask from level set, seeds from iterative vote and refined tensor field as gradient flow, watershed yields good results for segmenting every single cell.

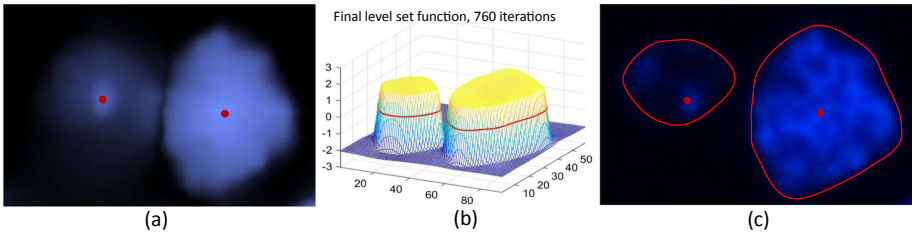

Fig. 7. Level set active contour movement till inward and outward balance, extract minimum energy line as final reconstructed cell contour. (a) Poisson reconstructed image from refined tensor field. (b) Final level set function after 760 iterations; (c) Final segmentation contour from level set evolution.

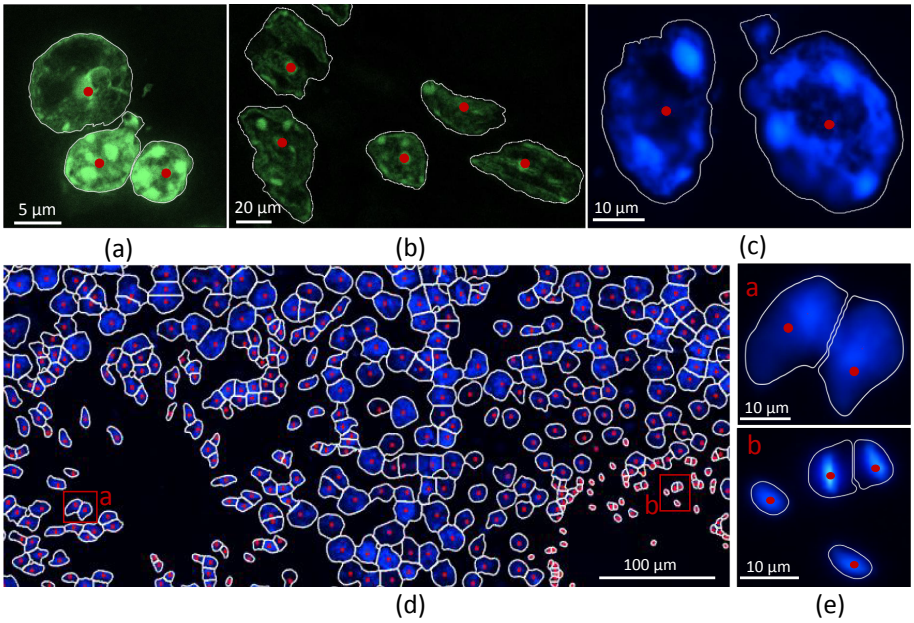

Fig. 8. Segmentation results. (a) Mouse brain STED image. (b) Mouse brain confocal image. (c) Mouse kidney expansion microscopy. (d–e) Mouse testicle expansion microscopy.

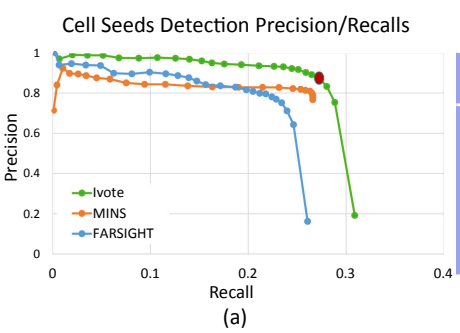

ExM Histology Segmentation DICE Scores & Standard Deviation comparison

Data Set	Method	DICE Scores	Standard Deviation
ExM Mouse Testicle Histology (1068*1068*7) 5796 cells	**LRPG (mine)**	**0.81**	**3.51%**
	LRPG without tensor refinement	0.67	9.02%
	FARSIGHT	0.61	13.20%
	MINS	0.67	14.21%
	TIMING 2.0	0.55	17.9%

(b)

Fig. 9. Analysis of segmentation results on ExM testicle images ($1068 \times 1068 \times 7$ pixels, 5,796 cells in total). (a) Precision-Recall curve comparison of seeds detection using iterative voting, FARSIGHT and MINS. (b) Segmentation DICE scores and standard deviation comparison.

2 Results Analysis

We quantified the results on seven ExM mouse testicle images ($1068 * 1068$) with 5796 cells in total. Seeds identification results are compared with MINS [13] and FARSIGHT [1] using precision-recall curves (Fig. 9a). Segmentation

results are quantified using DICE scores (Fig. 9b). LRPG yields significantly better results when segmenting sparsely-labeled cells with punctate features, where other methods over-segment the nuclei (Fig. 8a–c). LRPG also performs better when segmenting heterogeneous cells with a wide range sizes and contrasts (Fig. 9d–e).

3 Conclusion and Future Work

The proposed perceptual grouping approach is highly parallel and is extendable to higher-dimensional images, as well as multiplex imaging. Potential future directions include a GPU-based implementation to enable the practical segmentation of large images.

Acknowledgement. This work is funded in part by the National Institutes of Health/National Heart, Lung, and Blood Institute (NHLBI) #R01HL146745, the Cancer Prevention and Research Institute of Texas (CPRIT) #RR140013, the National Science Foundation I/UCRC BRAIN Center #1650566, and the National Institutes of Health Training Grant #T15LM007093.

References

1. Al-Kofahi, Y., Lassoued, W., Lee, W., Roysam, B.: Improved automatic detection and segmentation of cell nuclei in histopathology images. IEEE Trans. Biomed. Eng. **57**(4), 841–852 (2010)
2. Artur, C., Womack, T., Eriksen, J.L.J., Mayerich, D., Shih, W.C.: Hyperspectral expansion microscopy. In: 2017 IEEE Photonics Conference (IPC), pp. 23–24, October 2017
3. Beucher, S.: Watershed, hierarchical segmentation and waterfall algorithm. In: Serra, J., Soille, P. (eds.) Mathematical Morphology and Its Applications to Image Processing. Computational Imaging and Vision, vol. 2, pp. 69–76. Springer, Dordrecht (1994). https://doi.org/10.1007/978-94-011-1040-2_10
4. Chan, T.F., Shen, J., Vese, L.: Variational PDE models in image processing. Not. AMS **50**(1), 14–26 (2003)
5. Chen, F., Tillberg, P.W., Boyden, E.S.: Expansion microscopy. Science **347**(6221), 543–548 (2015)
6. Guy, G., Medioni, G.: Inferring global perceptual contours from local features. Int. J. Comput. Vis. **20**(1), 113–133 (1996). https://doi.org/10.1007/BF00144119
7. Heintzmann, R., Huser, T.: Super-resolution structured illumination microscopy. Chem. Rev. **117**(23), 13890–13908 (2017)
8. Huang, B., Babcock, H., Zhuang, X.: Breaking the diffraction barrier: super-resolution imaging of cells. Cell **7**(143), 1047–1058 (2010)
9. Huang, B., Bates, M., Zhuang, X.: Super resolution fluorescence microscopy. Annu. Rev. Biochem. **78**, 993–1016 (2009)
10. Jörgens, D., Moreno, R.: Tensor voting: current state, challenges and new trends in the context of medical image analysis. In: Hotz, I., Schultz, T. (eds.) Visualization and Processing of Higher Order Descriptors for Multi-Valued Data. MV, pp. 163–187. Springer, Cham (2015). https://doi.org/10.1007/978-3-319-15090-1_9

11. Li, C., Xu, C., Gui, C., Fox, M.D.: Distance regularized level set evolution and its application to image segmentation. IEEE Trans. Image Process. **19**(12), 3243–3254 (2010)
12. Loss, L., Bebis, G., Nicolescu, M., Skurikhin, A.: An iterative multi-scale tensor voting scheme for perceptual grouping of natural shapes in cluttered backgrounds. Comput. Vis. Image Underst. **113**(1), 126–149 (2009)
13. Lou, X., Kang, M., Xenopoulos, P., Muñoz-Descalzo, S., Hadjantonakis, A.K.: A rapid and efficient 2D/3D nuclear segmentation method for analysis of early mouse embryo and stem cell image data. Stem Cell Rep. **2**(3), 382–397 (2014)
14. Lu, H., et al.: TIMING 2.0: high-throughput single-cell profiling of dynamic cell-cell interactions by time-lapse imaging microscopy in nanowell grids. Bioinformatics **35**, 706–708 (2018)
15. Luo, J., Guo, C.E.: Perceptual grouping of segmented regions in color images. Pattern Recogn. **36**(12), 2781–2792 (2003)
16. Mordohai, P., Medioni, G.: Tensor voting: a perceptual organization approach to computer vision and machine learning. **2**(1), 1–136 (2006). Morgan & Claypool Publishers
17. Moreno, R., Garcia, M.A., Puig, D., Julià, C.: On adapting the tensor voting framework to robust color image denoising. In: Jiang, X., Petkov, N. (eds.) CAIP 2009. LNCS, vol. 5702, pp. 492–500. Springer, Heidelberg (2009). https://doi.org/10.1007/978-3-642-03767-2_60
18. Osher, S., Fedkiw, R.: Level Set Methods and Dynamic Implicit Surfaces, vol. 153. Springer, Heidelberg (2006). https://doi.org/10.1007/b98879
19. Rust, M.J., Bates, M., Zhuang, X.: Sub-diffraction-limit imaging by stochastic optical reconstruction microscopy (STORM). Nat. Methods **3**(10), 793–796 (2006)
20. Saadatifard, L., Abbott, L.C., Montier, L., Ziburkus, J., Mayerich, D.: Robust cell detection for large-scale 3D microscopy using GPU-accelerated iterative voting. Front. Neuroanat. **12**, 28 (2018)
21. Sahir, S.: Canny Edge Detection Step by Step in Python - Computer Vision, January 2019
22. Sethian, J.A.: Level Set Methods and Fast Marching Methods: Evolving Interfaces in Computational Geometry, Fluid Mechanics, Computer Vision, and Materials Science, vol. 3. Cambridge University Press, Cambridge (1999)
23. Shen, J., Jin, X., Zhou, C., Wang, C.C.L.: Gradient based image completion by solving the Poisson equation. Comput. Graph. **31**, 119–126 (2007)
24. Shtengel, G., et al.: Interferometric fluorescent super-resolution microscopy resolves 3D cellular ultrastructure. Proc. Nat. Acad. Sci. **106**(9), 3125–3130 (2009)
25. Vicidomini, G., Bianchini, P., Diaspro, A.: STED Super-resolved microscopy. Nat. Methods **15**(3), 173–182 (2018)
26. Willett, R.M., Harmany, Z.T., Marcia, R.F.: Poisson image reconstruction with total variation regularization. In: 2010 IEEE International Conference on Image Processing, pp. 4177–4180, September 2010. https://doi.org/10.1109/ICIP.2010.5649600

DISCo: Deep Learning, Instance Segmentation, and Correlations for Cell Segmentation in Calcium Imaging

Elke Kirschbaum[1,2(✉)], Alberto Bailoni[1], and Fred A. Hamprecht[1]

[1] Interdisciplinary Center for Scientific Computing (IWR), Heidelberg University, 69120 Heidelberg, Germany
{alberto.bailoni,fred.hamprecht}@iwr.uni-heidelberg.de
[2] Amazon Research, 72076 Tübingen, Germany
elkeki@amazon.com

Abstract. Calcium imaging is one of the most important tools in neurophysiology as it enables the observation of neuronal activity for hundreds of cells in parallel and at single-cell resolution. In order to use the data gained with calcium imaging, it is necessary to extract individual cells and their activity from the recordings. We present DISCo, a novel approach for the cell segmentation in calcium imaging videos. We use temporal information from the recordings in a computationally efficient way by computing correlations between pixels and combine it with shape-based information to identify active as well as non-active cells. We first learn to predict whether two pixels belong to the same cell; this information is summarized in an undirected, edge-weighted graph which we then partition. Evaluating our method on the Neurofinder public benchmark shows that DISCo outperforms all existing models trained on these datasets.

Keywords: Calcium imaging · Cell segmentation · Neuro imaging analysis

1 Introduction

Calcium imaging is a microscopy technique that allows the observation of the activity of large neuronal populations at single-cell resolution [3,8,13]. This makes it one of the most important tools in neurophysiology since it enables the study of the formation and interaction of neuronal networks in the brain. The data recorded with calcium imaging is a sequence of images that shows multiple cells at fixed locations and with varying luminosity. The extraction of

E. Kirschbaum—This work was done while E.K. was at 1.

Electronic supplementary material The online version of this chapter (https://doi.org/10.1007/978-3-030-59722-1_15) contains supplementary material, which is available to authorized users.

A. L. Martel et al. (Eds.): MICCAI 2020, LNCS 12265, pp. 151–162, 2020.
https://doi.org/10.1007/978-3-030-59722-1_15